Photoacoustics 22 (2021) 100263

Contents lists available at ScienceDirect

Photoacoustics

journal homepage: www.elsevier.com/locate/pacs

Croconaine-based nanoparticles enable efficient optoacoustic imaging of murine brain tumors

Nian Liu [a,b], Vipul Gujrati [a,b,*], Jaber Malekzadeh-Najafabadi [a], Juan Pablo Fuenzalida Werner [b], Uwe Klemm [b], Longguang Tang [c], Zhenyue Chen [d], Jaya Prakash [b,e], Yuanhui Huang [a,b], Andre Stiel [b], Gabriele Mettenleiter [f], Michaela Aichler [f], Andreas Blutke [f], Axel Walch [f], Karin Kleigrewe [g], Daniel Razansky [d], Michael Sattler [h,i], Vasilis Ntziachristos [a,b,*]

[a] Chair of Biological Imaging, Center for Translational Cancer Research (TranslaTUM), School of Medicine, Technical University of Munich, Munich 81675, Germany
[b] Institute of Biological and Medical Imaging, Helmholtz Zentrum München (GmbH), Neuherberg 85764, Germany
[c] State Key Laboratory of Molecular Vaccinology and Molecular Diagnostics & Center for Molecular Imaging and Translational Medicine, School of Public Health, Xiamen University, Xiamen 361005, China
[d] Institute for Biomedical Engineering and Institute of Pharmacology and Toxicology, University of Zurich and ETH Zurich, Zurich 8093, Switzerland
[e] Department of Instrumentation and Applied Physics, Indian Institute of Science, C. V. Raman Road, Bengaluru 560012, India
[f] Research Unit Analytical Pathology, Helmholtz Zentrum München (GmbH), Neuherberg 85764, Germany
[g] Bavarian Center for Biomolecular Mass Spectrometry (BayBioMS), Technical University of Munich, Freising 85354, Germany
[h] Bavarian NMR Center and Center for Integrated Protein Science Munich, Department of Chemistry, Technical University of Munich, Garching 85747, Germany
[i] Institute of Structural Biology, Helmholtz Zentrum München (GmbH), Neuherberg 85764, Germany

ARTICLE INFO

Keywords:
Brain tumor
Croconaine
Nanoparticles
Optoacoustic (photoacoustic) imaging
MSOT

ABSTRACT

Contrast enhancement in optoacoustic (photoacoustic) imaging can be achieved with agents that exhibit high absorption cross-sections, high photostability, low quantum yield, low toxicity, and preferential bio-distribution and clearance profiles. Based on advantageous photophysical properties of croconaine dyes, we explored croconaine-based nanoparticles (CR780RGD-NPs) as highly efficient contrast agents for targeted optoacoustic imaging of challenging preclinical tumor targets. Initial characterization of the CR780 dye was followed by modifications using polyethylene glycol and the cancer-targeting c(RGDyC) peptide, resulting in self-assembled ultrasmall particles with long circulation time and active tumor targeting. Preferential bio-distribution was demonstrated in orthotopic mouse brain tumor models by multispectral optoacoustic tomography (MSOT) imaging and histological analysis. Our findings showcase particle accumulation in brain tumors with sustainable strong optoacoustic signals and minimal toxic side effects. This work points to CR780RGD-NPs as a promising optoacoustic contrast agent for potential use in the diagnosis and image-guided resection of brain tumors.

1. Introduction

Optoacoustic imaging is a versatile imaging tool that is highly applicable in preclinical research. It offers the ability to visualize organs or tissues with high contrast and high spatial resolution, and quantify sub-organ structures at a depth of centimeters [1]. Multispectral optoacoustic tomography (MSOT) enables functional and molecular imaging by illuminating tissue at multiple wavelengths and processing these images to resolve the distribution of different photo-absorbing moieties by identifying their different absorption spectral profiles, yielding the biodistribution of reporter molecules and tissue biomarkers [2]. MSOT exhibits marked advantages over other imaging techniques, such as the absence of harmful ionizing radiation, and the unique scalability of spatial resolution and depth penetration across both optical and ultrasonic dimensions [3]. A variety of molecules that yield strong optoacoustic signals include endogenous hemoglobin, melanin, lipids, collagen, and exogenously delivered synthetic contrast agents [4]. Several label-free optoacoustic imaging applications have been showcased using endogenous chromophores for contrast generation [4]. Using hemoglobin for example, optoacoustic imaging was used to

* Corresponding authors at: Chair of Biological Imaging, Center for Translational Cancer Research (TranslaTUM), School of Medicine, Technical University of Munich, Munich 81675, Germany.
E-mail addresses: vipul.gujrati@tum.de (V. Gujrati), v.ntziachristos@tum.de (V. Ntziachristos).

https://doi.org/10.1016/j.pacs.2021.100263
Received 11 December 2020; Received in revised form 24 February 2021; Accepted 11 March 2021
Available online 23 March 2021

visualize angiogenesis, tissue oxygenation, inflammation, and metabolic processes [5–9]. However, to enable significantly richer profiling of biological activities, there is a need for additional low-cost agents that are versatile and easy to synthesize or structurally modify [2].

A successful optoacoustic agent should have a molar absorption coefficient, high optoacoustic generation efficiency (OGE), low quantum yield, and a narrow spectral profile for more accurate and sensitive spectral unmixing [10]. Furthermore, optoacoustic imaging agents should be photostable, target-specific, biocompatible, and minimally toxic in order to be applicable in imaging research [10]. A range of organic and inorganic contrast agents has previously been explored for optoacoustic contrast enhancement [11,12]. Metal-based inorganic contrast agents have demonstrated strong absorption contrast, but undergo physicochemical and biochemical changes such as reshaping, fragmentation, and aggregation upon light irradiation, resulting in poor photostability and altered optical behavior [13]. Moreover, long-term toxic side effects remain a concern for metallic agents due to low biocompatibility and long deposition time in the body after systemic administration [14]. Organic dyes can overcome the challenges of inorganic agents, as their chemical structures can be easily modified, and they often exhibit good biocompatibility, easy metabolism, and low toxicity [15]. However, due to low aqueous solubility, rapid systemic clearance, and non-specificity toward cancers, most of the organic dyes cannot be used for systemic administration.

To improve bioavailability, we have previously demonstrated that encapsulation of organic dyes, or chemical conjugation or modification with biodegradable polymers and peptides, results in nanoparticles with enhanced systemic circulation and cancer-specific targeting ability [1,16,17]. In particular, we proposed an encapsulation strategy to utilize the US Food and Drug Administration (FDA)-approved indocyanine green (ICG) for optoacoustic imaging [17]. ICG is a cyanine dye with a high absorption cross-section but poor photostability and rapid renal clearance. We demonstrated that encapsulation of ICG into PEGylated liposomes (DOXIL lipid formulation) results in a higher absorption cross-section, better photostability, and enhanced circulation time, making these nanoparticles optimal for optoacoustic imaging [17]. Furthermore, we have recently reported that when fluorescent dyes (iBu-TSBSH5) are encapsulated into nanoparticles, the Förster Resonant Energy Transfer (FRET) effect on these dyes can result in self-quenching of the fluorescence signal, making them suitable for optoacoustic imaging [16]. Moreover, various near-infrared (NIR)-absorptive organic dyes with different backbones have been developed and loaded into nanoparticles to enhance the bioavailability and optoacoustic signals in deep tissue. Dyes such as squaraine [18,19], and BODIPY [20] exhibit a sharp absorption peak, but their high quantum yields make them much better suited for fluorescence imaging. Tetrapyrole structures such as porphyrin and phthalocyanines are widely used as photodynamic therapy (PDT) agents in treating cancers [21]. However, these structures have poor aqueous solubility and low molar extinction coefficients and therefore generate lower optoacoustic signals [15].

In search for improved optoacoustic agents, we herein examined the properties of organic dyes with croconaine backbones and their derivatives which exhibit narrow, strong absorption coefficients in the NIR region, are exceptionally stable chemically, photochemically, and thermally, and can be easily modified chemically [22]. Croconaine dyes have been widely used in organic electronic devices and analytic chemistry applications [23–25]. The use of nanoparticle formulations promises to improve the inherent properties of croconaine dyes that normally limit their preclinical *in vivo* applications, including low aqueous solubility, inability to actively target cancer cells, and a short half-life. Several studies have reported optoacoustic imaging applications of croconaine dyes encapsulated into such nanoparticle formulations [26]. For example, nanoparticle formulations were used to optimize physicochemical properties of croconaine dyes, such as croconaine rotaxane incorporated into stealth liposomes for acid-activated photothermal heating and ratiometric optoacoustic imaging at acidic pH [27]. Another group developed albumin-croconaine nanoparticles for pH-based optoacoustic imaging of tumors [28]. Furthermore, PEGylated croconaine dyes (CR780) were developed for targeted imaging of subcutaneous breast cancer tumors [29]. All these croconaine formulations were designed to demonstrate the optoacoustic imaging applications of croconaine dyes using subcutaneously implanted tumors that are relatively easy to target. Finally, Liu et al. reported a NIR-II croconaine dye encapsulated into a viral vector to form nanoparticles for targeted *in vivo* orthotopic brain tumor imaging, although *in vivo* safety of such viral nanoparticles is still to be thoroughly evaluated [30].

One particularly challenging target for nanoparticle contrast agents is tumors in the brain because of the blood brain barrier (BBB) and blood tumor barrier (BTB) [31,32]. The BBB is a physical barrier mainly formed by endothelial cells in brain capillary walls and tight junctions which maintains and protects the sensitive environment of the brain [33]. The BBB moreover plays a significant metabolic role by disposing waste products, metabolizing chemicals and toxins, and markedly limiting the uptake of theranostic drugs in the brain [34]. Tumor growth and progression compromises the integrity of the BBB, and such a disrupted BBB is referred as the blood tumor barrier (BTB) [33], which is characterized by a heterogeneous permeability of small and large molecules. The passive delivery of nanoparticles of appropriate size (20−70 nm) to the brain tumor is considered optimal [31,35]. Although several optoacoustic agents (such as gold nanoparticles [36,37], MoS_2 nanosheets [38,39], and semiconducting polymeric nanoparticles [40]) have been reported for optoacoustic imaging of deep brain tumors, their biodegradability remains a major concern. Therefore, biocompatible nanoparticles with suitable size and high optoacoustic generation efficiency for deep brain tumor imaging are highly desirable.

To this end, we conjugated the croconaine backbone-derived CR780 dye with a NH_2-PEG_{2000}-MAL and the cancer-targeting c(RGDyC) peptide to generate self-assembled nanoparticles with the ability to actively target a brain tumor and enable longitudinal optoacoustic imaging. We sought to test the tumor-targeting efficacy of these nanoparticles under the most challenging delivery conditions, and ultimately applied them to the imaging of an orthotopic brain tumor model using MSOT (Scheme 1). First, we compared CR780RGD-NPs to the free CR780 dye and the gold industry standard FDA-approved dye ICG in order to show that the physicochemical properties of the nanoparticles (molar absorptivity, OGE, and photostability) are optimal for effective application in optoacoustic imaging. Next, we tested the ability of MSOT to detect localized croconaine nanoparticles *in vitro* using tissue-mimicking phantoms at depths and beyond that of a mouse brain tumor. We also tested the *in vitro* BBB penetration capability and cell uptake of these nanoparticles. We further imaged a standard subcutaneous tumor model using CR780RGD-NPs and control non-targeted groups (CR780RAD-NPs) to evaluate whether the c(RGDyC) peptide-functionalized nanoparticles exhibit active targeting. Finally, the CR780RGD-NPs and CR780RAD-NPs were systemically injected into a mouse brain tumor model to evaluate the ability of the nanoparticles to penetrate the BTB and generate localized contrast from the tumor site. Optoacoustic images of the isolated brain and hematoxylin-eosin (H&E) staining of brain slices were used to confirm the presence of CR780RGD-NPs in the brain tumor, even after 24 h. This study establishes ultrasmall particles based on croconaine dyes as comprehensive preclinical contrast agents which are photostable, and simple to manufacture and functionalize for enhanced tumor targeting. Furthermore, our biosafety study suggests that CR780RGD-NPs are safe for preclinical *in vivo* application.

2. Materials and methods

2.1. Materials

C(RGDyC) peptide and C(RADyC) peptide were bought from GL biochem (Shanghai, China), NH_2-PEG_{2000}-SH were bought from Creative PEGWorks (Chapel Hill, USA). ICG, IR780 iodide, IR820, and 3-(4,5-

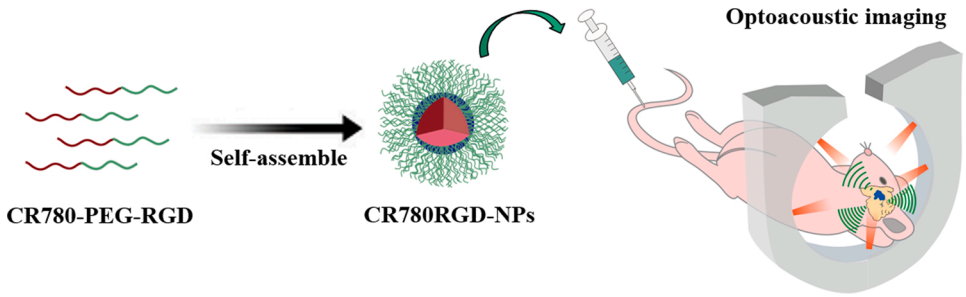

Scheme 1. Schematic of the CR780RGD-NPs synthesis and optoacoustic imaging of a brain tumor.

dimethylthiazol-2-yl)-2,5-diphenyl-tetrazolium bromide (MTT) were purchased from Sigma-Aldrich (Munich, Germany). IRDye800CW NHS Ester was bought from LI-COR Biosciences (Nebraska, USA). Other chemical reagents were obtained from TCI Deutschland GmbH (Eschborn, Germany).

2.2. Materials characterization

^{1}H NMR spectrum was recorded on a Bruker spectrometer at 500 MHz. The *m/z* ratios of the compounds were measured with a MALDI UltrafleXtreme (Bruker) using dihydroxybenzoic acid as matrix. The molar absorption coefficient and quantum yield of dyes were calculated as previously described [41]. For the quantum yield measurement, three concentrations of dyes in ethanol (absorbance below 0.1) were prepared and corresponding fluorescence intensity was evaluated, then the fluorescence intensity was plotted against absorbance and fitted into a linear function. As the quantum yield of ICG (in ethanol) is 0.05, then the quantum yield of other agents were calculated as follows: $Slope_{dyes}/Slope_{ICG}$*0.05 ($Slope_{ICG}$ = 5166) [42]. The nanoformulations in water were characterized by transmission electron microscopy (Zeiss Libra 120 Plus, Carl Zeiss NTSb GmbH, Oberkochen, Germany) and Malvern Zetasizer. Absorption spectra were measured with UV-1800 spectrometer (Shimadzu, Japan). Optoacoustic spectra were collected by an MSOT inVision 256-TF (iThera Medical, Munich, Germany) measurement and further correction with India ink, Brilliant Black BN (BBN) [43]. Briefly, the Indian ink was used to correct the known pulse-to-pulse fluctuations from the OPO laser. The BBN was selected as a reference due to its photostability, and lack of any fluorescence generation allowed us to assign an OGE value of 1.0, assuming no decay channels taking place. The OGE of samples is equal to the slope of the line where corrected optoacoustic intensities are plotted against absorbance [43,44]. The photostability of samples was measured using an MSOT inVision 256-TF with pulsed laser irradiation (fluence 10 mJ/cm^2, 10 Hz pulse repetition rate, 1 h).

2.3. Synthesis of CR780, CR780-PEG-RAD, and CR780-PEG-RGD

CR780 was synthesized according to a previously reported method [45]. ^{1}H NMR (500 MHz, DMSO-d_6) δ8.52 (s, 2 H), 7.03 (d, *J* =6 Hz, 2 H), 3.99 (d, *J* =16.6 Hz, 4 H), 3.52 (t, *J* =14.1 Hz, 5 H), 2.73 – 2.60 (m, 2 H), 2.04 (d, *J* =12.9 Hz, 4 H), 1.73 (q, *J* =13.3 Hz, 4 H). MALDI: *m/z* = 529.183 [M + H]$^+$. CR780-PEG-RAD or CR780-PEG-RGD was synthesized by esterification. Briefly, CR780 (0.1 mmol), EDC·HCl (0.12 mmol), NHS (0.12 mmol) were dissolved in 2 mL of DMF. The mixture was stirred for 2 h, followed by the addition of NH_2-PEG_{2000}-SH (0.1 mmol). After stirring at room temperature for 24 h, CR780-PEG-SH was purified by reversed-phase HPLC column. Then CR780-PEG-SH was reacted with c(RADyC) or c(RGDyC) peptide (0.1 mmol) under slightly acidic condition for 2 h. CR780-PEG-RAD or CR780-PEG-RGD were purified by reverse-phase HPLC column and then dry-freezing.

2.4. Preparation of CR780RAD-NPs and CR780RGD-NPs

CR780-PEG-RAD (1 mg), or CR780-PEG-RGD (1 mg) was dissolved in deionized water (1 mL) and sonicated for 5 min, obtaining uniform-sized CR780RAD-NPs, or CR780RGD-NPs.

2.5. Penetration depth estimation

Tissue-mimicking cylindrical phantoms with different radii were made by using the mixture of intralipid (2 mL), agar (2 g), India ink solution (98 mL, absorbance 0.15 at 780 nm) [46,47]. Then tubing containing different concentration of CR780RGD-NPs was inserted into the tissue-mimicking phantoms for optoacoustic detection from different depths using an MSOT inVision 256-TF. *In vivo* penetration depth experiments were done by injecting CR780RGD-NPs (5 μM) in the mouse brains using small Hub RN needle (Hamilton, Timis, Romania) (bregma +1.0 mm, left lateral 2.0 mm and depth 5.0 mm). The optoacoustic signal was subsequently measured using an MSOT inVision 256-TF.

2.6. In vitro BBB penetration capability

The *in vitro* BBB model was constructed to explore the BBB permeability of nanoparticles [48,49]. Briefly, 10^5 of HBEC-5i cells were cultured with multiple layers on a Transwell filter system (pore size 0.4 μm). CR780-derived nanoparticles (50 μM) were added into the apical chamber for 4 h's incubation at 37 °C, then the medium in the basolateral chambers was collected to measure the absorption intensities at 780 nm. As the absorption intensity of CR780-derived nanoparticles has a linear relationship with the concentrations of NPs, the transport efficiency of NPs was calculated by dividing the weight of NPs in the basolateral chamber by the weight of 50 μM NPs [50].

2.7. In vitro experiments

U87MG cells were sub-cultured in a 96-well plate at a density of 1 × 10^4 cells/well overnight. The cells were treated with different concentrations of CR780RAD-NPs and CR780RGD-NPs for 24 h. Then the cell viability was measured by MTT assay to check the cytotoxicity of nanoparticle samples.

Cellular internalization was used to assess targeting by c(RGDyC) peptide-modified nanoparticles. A total of 1 × 10^4 of cells were seeded on glass dishes at 37 °C in a 5% CO_2 atmosphere and cultured for 24 h. Then CR780RAD-NPs or CR780RGD-NPs (50 μM) were added to the dishes and incubated for 4 h. The cells were thoroughly rinsed with PBS three times. Cellular uptake was observed based on fluorescence signal from CR780 based nanoparticles by Leica DMI3000 B Inverted Microscope (Wetzlar, Germany).

2.8. Brain tumor mouse model

All procedures involving animal experiments were approved by the

Government of Upper Bavaria. Subcutaneous U87MG tumor models were prepared by subcutaneously implanting a suspension of 2×10^6 U87MG cells into nod scid shorn mice (6 weeks). The orthotopic tumor models were prepared using nod scid shorn mice (6 weeks). U87MG cells (4×10^5) in PBS (3 μL) were implanted into the mouse striatum (bregma +1.0 mm, left lateral 2.0 mm, and depth 3.0 mm). The brain imaging was conducted four weeks after implantation [51].

2.9. In vivo MSOT imaging

Mice bearing brain tumors were anesthetized by 1% isoflurane delivered via a nose cone, and then 100 μL of CR780RAD-NPs or CR780RGD-NPs (1 mM) were injected via the tail vein. *In vivo* optoacoustic images were acquired at different time points before and after injection (0, 4, 24 h). The MSOT (MSOT256-TF, iThera Medical GmbH, Munich, Germany) scanning was carried out from 680 to 900 nm with a step size of 10 nm and 10 signal averages. The light was illuminated on the sample uniformly from 5 different directions using a one to ten (five pairs) fiber bundle. The generated acoustic signals were acquired using a 256-element transducer array (5 MHz center frequency) with 270-degree angle coverage and 40 Ms/sec DAQ sampling rate. This acquired sinogram data was initially filtered using a Chebyshev filter having the bandwidth as 0.1−8 MHz. The filtered sinogram data was used to reconstruct the mice/phantom image using a model-based reconstruction with a least squares QR inversion method running for 100 iterations. The model-based reconstruction was performed at all the wavelengths i.e. 680 nm–900 nm with a step size of 10 nm. The reconstructed images were used to detect the CR780 signal using the CR780 reference spectral information, the CR780 signal was detected using linear regression approach (unmixing method) [44]. The averaged optoacoustic signals of brain tumor regions were extracted using ViewMSOT 4.0 software (iThera Medical, Munich).

2.10. Ex vivo optoacoustic imaging, fluorescence imaging, and histological analysis

The mice were sacrificed at 24 h post-injection and the brain, kidney, heart, liver, and spleen were isolated and scanned by MSOT. Isolated brains were fixed and frozen in OCT embedding gel. The tissue blocks were sectioned in the axial dimension, at a 300 mm micron pitch, and bright field as well as fluorescence images were recorded from each slice using a fluorescence cryosectioning imaging (FCSI) system. The FCSI system is based on a cryotome (CM 1950, Leica Microsystems, Wetzlar, Germany), fitted with a motorized spectral illumination and multispectral CCD-based detection in epi-illumination mode. The cryosection slices were captured on glass slides. The slides obtained were stained by H&E and imaged with a light microscope (Carl Zeiss).

2.11. In vivo pharmacokinetics studies

Healthy C57BL/6 mice were intravenously injected with 100 μL of CR780RGD-NPs (1 mM). Blood was collected from the mouse heart at different time points (15 min, 1 h, 2 h, 4 h, 8 h, 12 h, and 24 h), and then serum was separated by centrifugation using serum separator tubes (Sarstedt AG &Co.). Absorption intensities of nanoparticles in serum samples were measured by a UV-1800 spectrometer (Shimadzu, Japan). Pharmacokinetic parameters were calculated with non-compartmental analysis using WinNonlin 4.1 software (Pharsight Corp., Palo Alto, CA, USA).

2.12. Blood hematology and biochemistry analyses

C57BL/6 mice were randomly divided into 4 groups (5 mice per group). The control group was i.v. injected with 100 μL of PBS buffer, and the other 3 groups were i.v. injected with 100 μL of CR780RGD-NPs (1 mM). On days 1, 7, and 14, blood from CR780RGD-NPs treated group was sampled. From the control group, blood was sampled on day 14. The blood samples were then used for hematology and blood biochemistry test using Hitachi 917 Clinical Chemistry Analyzer (Roche, Germany).

2.13. Statistics

Sample sizes were chosen based on the literature. Animals of the same gender, age, and genetic background were randomized for grouping. Results were expressed as mean ± SD. Statistical analyses were performed using OriginPro 8 (Northampton, Massachusetts, USA). Inter-group differences were assessed for significance using One-Way ANOVA with Tukey's HSD test.

3. Results

3.1. Synthesis and characterization of CR780

Croconaines are pseudooxocarbon dyes derived from croconic acid [22]. For facile polymeric conjugation, we previously synthesized a croconaine dye with two carboxyl groups referred to as CR780 [45]. CR780 was prepared by a three-step reaction (nucleophilic substitution, condensation, and ester hydrolysis) as shown in Fig. S1. Fig. S2, S3 show the ^{1}H-NMR spectrum and mass spectrum of CR780, which confirmed the right compound. Table S1 shows the experimental comparison of the photophysical properties of CR780 with previously reported optoacoustic dyes (ICG, IRDye800CW, IR780 iodide, and IR820) in ethanol [52–54]. Comparison data shows that CR780 has a strong absorption peak at 780 nm and a NIR fluorescence emission peak at 800 nm. CR780 exhibits a molar absorption coefficient significantly higher than ICG and other dyes and a much smaller quantum yield (88 % less than ICG). We further experimentally compared the OGE of CR780 with ICG, IRDye800CW, IR780 iodide, and IR820. The slope value at each point indicates the OGE, the ratio of optoacoustic intensity and absorbance. OGE values indicate that ability of the compound to convert optically absorbed energy into pressure waves that give a strong optoacoustic signal. Fig. S4 shows that CR780 exhibits a much higher optoacoustic intensity compared with the other dyes. Our results clearly show that CR780 exhibits an OGE that is 1.79 times higher than IR820, 1.85 times higher than ICG, 3.29 times higher than IRDye800CW, and 8.5 times higher than IR780 iodide. Based on the high molar absorption coefficient and OGE, we set out to use the CR780 to prepare ultrasmall, self-assembled nanoparticles that are suitable for brain tumor targeted imaging.

3.2. Synthesis and characterization of CR780RGD-NPs

We conjugated the hydrophobic CR780 to the hydrophilic NH_2-PEG_{2000}-SH and c(RGDyC) peptide to generate nanoparticles that can self-assemble based on hydrophobic and hydrophilic interactions [55]. The c(RGDyC) peptide is used to target $\alpha_v\beta_3$ integrin receptors, which are expressed on activated endothelial cells of the tumor neovasculature and tumor cells [56]. In parallel, as controls for the tumor-targeting ability of the nanoparticles, we prepared CR780RAD-NPs. Fig. S5,S6 shows the CR780-PEG-RGD synthesis steps and corresponding MALDI-TOF analyses indicating the purity of the compounds. Based on the hydrophilic and hydrophobic interactions, CR780RGD-NPs can be formulated after a brief sonication in water. Fig. 1a shows that the self-assembled CR780RGD-NPs generate a clear green, homogeneous aqueous solution. We evaluated the shape and size of the nanoparticles using transmission electron microscopy (TEM) and dynamic light scattering (DLS). Fig. 1b and Fig. S7 show that the CR780RGD-NPs exhibit circular morphology with an average size of approximately 25 nm. The control group from CR780RAD-NPs show a similar size distribution (Fig. S8). Fig. 1c,d show the optical and optoacoustic spectrum of CR780RGD-NPs, which have a narrow and intense peak at 780 nm, similar to CR780RAD-NPs (Fig. S9). The zeta potential of

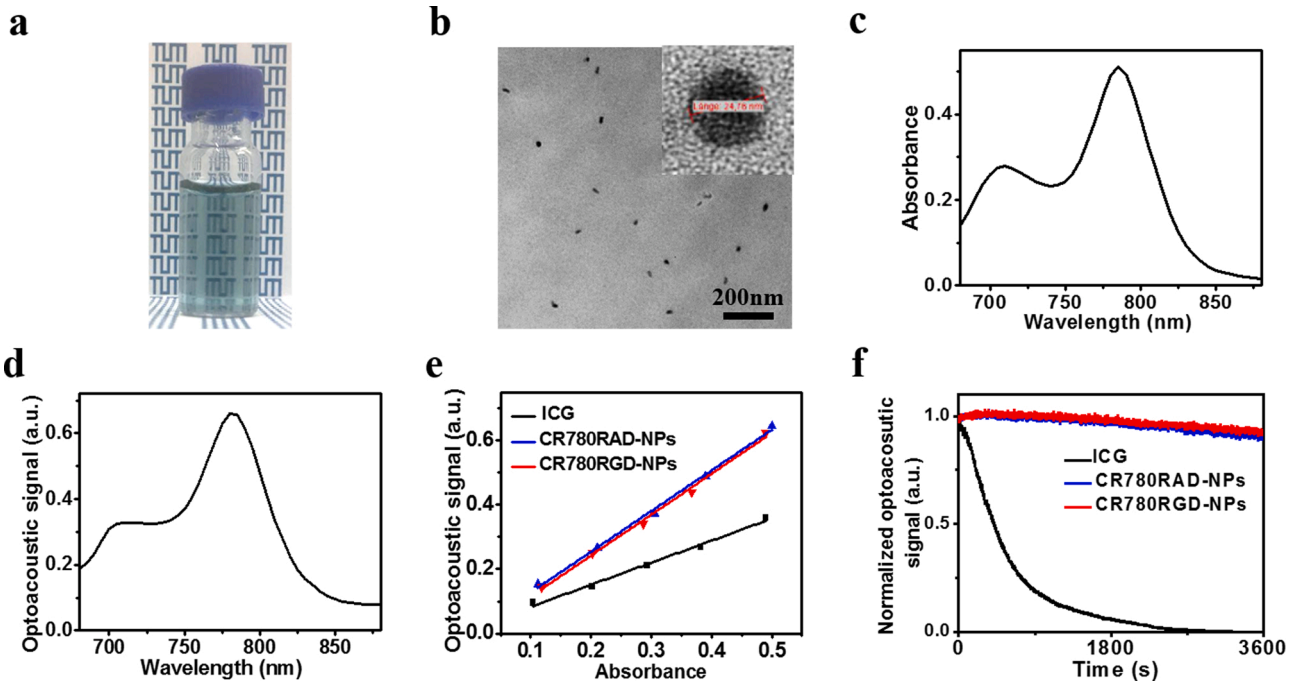

Fig. 1. (a) CR780RGD-NPs in deionized water. (b) TEM image of CR780RGD-NPs. (c) Optical spectrum of CR780RGD-NPs. (d) Optoacoustic spectrum of CR780RGD-NPs. (e) Optoacoustic signal intensity of ICG, CR780RAD-NPs, and CR780RGD-NPs at different absorbance. (f) Optoacoustic signal changes of ICG, CR780RAD-NPs, and CR780RGD-NPs after pulsed laser irradiation (fluence 10 mJ/cm^2, 10 Hz pulse repetition rate, 1 h).

CR780RAD-NPs and CR780RGD-NPs are -16.9 mV and -17.2 mV, respectively (on day 0, Fig. S10). We measured the absorbance intensities, particle size, and zeta potential of CR780-derived nanoparticles for 14 days (Fig. S11), with no significant changes recorded. Next, we compared the quantum yield and OGE of CR780 and CR780RGD-NPs in the water phase, where CR780RGD-NPs had a 2.33-fold higher quantum yield and a 1.63-fold higher OGE than CR780, as PEGylation and self-assembly improve the dispersibility of hydrophobic CR780 (Fig. S12) [29,44]. We then compared the OGE of CR780-derived nanoparticles with ICG in 10 % FBS due to the instability

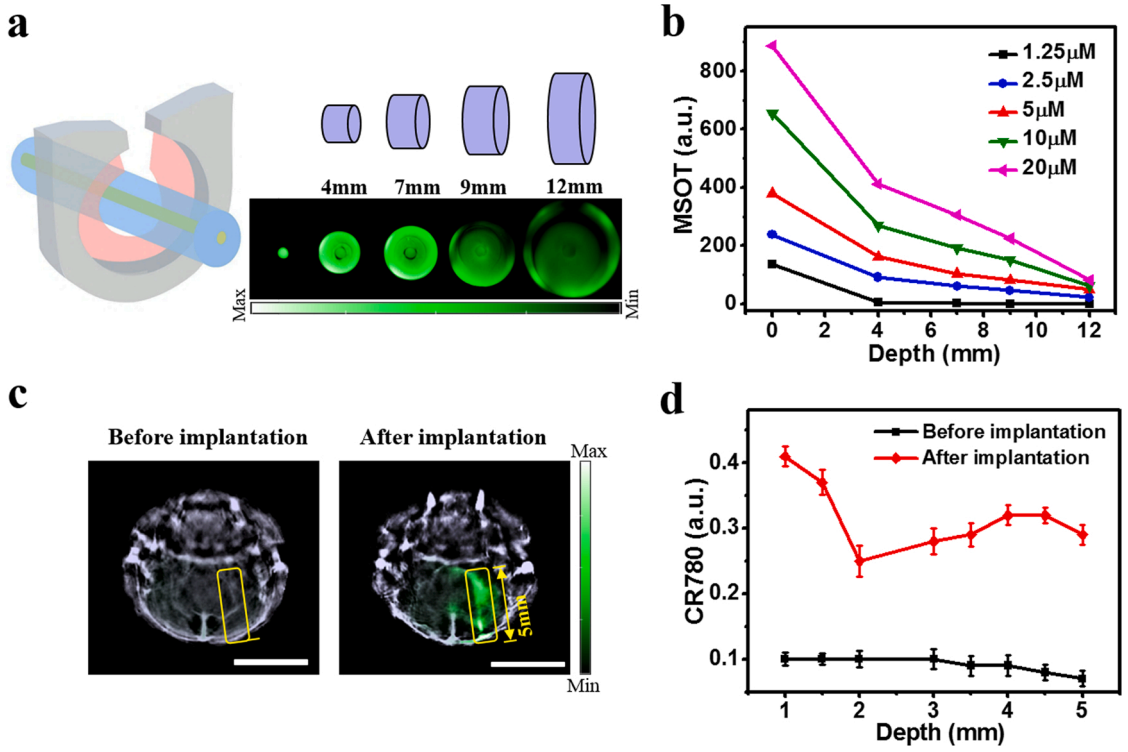

Fig. 2. (a) Optoacoustic imaging of tissue-mimicking phantoms of increasing thickness containing 5 μM CR780RGD-NPs at 780 nm. (b) Optoacoustic intensities of different concentration of CR780RGD-NPs from phantoms of different thicknesses. (c) Unmixed MSOT imaging of a mouse brain before and after injection of CR780RGD-NPs (5 μM). Scale bar, 5 mm. (d) Optoacoustic intensity of ROI at different depths *in vivo*.

of ICG in the water phase. Fig. 1e shows a much higher slope value for CR780RAD-NPs and CR780RGD-NPs than for ICG. The calculated OGE value was 1.85 times higher for CR780-derived nanoparticles than for ICG, indicating that both nanoformulations are suitable for optoacoustic imaging. We further evaluated the photostability of CR780RGD-NPs by continuously irradiating the samples with a pulsed laser (fluence 10 mJ/cm^2) for 1 h and compared the changes in optoacoustic intensity against ICG. Fig. 1f shows that CR780RAD-NPs and CR780RGD-NPs remained unbleached, whereas ICG was completely bleached under the same irradiation conditions. These results of the characterization studies clearly indicate that CR780RGD-NPs are ultrasmall (average particle size 25 nm) and can generate strong optoacoustic signals. The optimal physicochemical properties of CR780RGD-NPs make them suitable for *in vivo* optoacoustic imaging of orthotopic brain tumors.

3.3. Optoacoustic imaging with CR780RGD-NPs at different depths in vitro and in vivo

To explore the potential of CR780RGD-NPs for deep tissue imaging, we assessed the optoacoustic imaging depth at 780 nm using tissue-mimicking phantoms. Cylindrical phantoms of agar containing India ink were prepared to fit within a commercially available MSOT system, and tubing filled with different concentration of CR780RGD-NPs was placed in the center. Various phantoms were created with different radii to examine the imaging of nanoparticles at different depths. Fig. 2a shows the optoacoustic images of tissue-mimicking phantoms of increasing thickness; the optoacoustic signal of CR780RGD-NPs placed in the tubing was monitored from the center. Fig. 2b and Fig. S13 show that CR780RGD-NPs contrast levels correlated with phantom thickness and nanoparticle concentration. Detection limits are also defined in the context of lesion concentration, lesion size and depth [57], thus the lower detection limit of the unmixing method for CR780RGD-NPs at depths of 7 mm or 9 mm in tissue-mimicking phantoms was found to be 1.25 μM. Optoacoustic contrast due to CR780RGD-NPs was visible at different depths, confirming the potential for the optoacoustic detection of CR780RGD-NPs from deep brain tumors.

To examine whether CR780RGD-NPs could generate strong optoacoustic signals at different depths within tumors *in vivo*, despite background noise due to endogenous contrast agents like blood and reflections at the skull, we injected CR780RGD-NPs into a mouse brain at a depth of 5 mm. Fig. 2c shows the unmixed optoacoustic images of the mouse brain before and after implantation of CR780RGD-NPs. A strong optoacoustic signal from the implanted CR780RGD-NPs at different depths in the brain was evident. Fig. 2d shows no variation in optoacoustic intensity across different depths in animals prior to nanoparticles implantation, whereas the optoacoustic intensity was approximately 3.5 times higher at a 5 mm depth after CR780RGD-NP implantation. These results clearly indicate that upon uptake and accumulation in the brain tumor, the CR780RGD-NPs can generate a strong optoacoustic signal easily detectable over background noise from the skull, blood, and brain tissue.

3.4. In vitro BBB penetration capability and cell uptake

We next carried out an *in vitro* BBB penetration test using HBEC-5i (human brain microvascular endothelial cell line) derived BBB model (Fig. S14). HBEC-5i cells were cultured with multiple layers on a Transwell filter system (pore size 0.4 μm) [49]. CR780-derived nanoparticles (50 μM) were added into the apical chamber, and the absorbance of the solution in apical chambers and basolateral chambers was evaluated at 4 h to calculate the transport efficiency. The results show that the transmembrane transport efficiency of nanoparticles was 10.9 ± 1.2 %, 11.8 ± 1% for CR780RAD-NPs, CR780RGD-NPs, respectively. These results indicate that such ultrasmall particles might also be able to penetrate through the disease-compromised BTB *in vivo*. Next we tested the *in vitro* active targeting ability of CR780RGD-NPs using U87MG cells (glioblastoma cell line). Uptake of non-targeted CR780RAD-NPs and integrin $\alpha_v\beta_3$-targeted CR780RGD-NPs by U87MG cells were monitored by fluorescence microscopy after 4 h treatment with nanoparticles. Cells treated with CR780RGD-NPs showed a stronger fluorescence signal than those treated with the non-targeting groups (Fig. S15). We further evaluated the cytotoxic effects of nanoparticles in U87MG cells by treating them with different concentrations of CR780RAD-NPs and CR780RGD-NPs for 24 h. An MTT assay for assessing cell metabolic activity showed no appreciable cytotoxicity (Fig. S16).

3.5. In vivo optoacoustic imaging of a brain tumor

To test the ability of CR780RGD-NPs to specifically accumulate in a brain tumor, we first subcutaneously implanted U87MG cells and subsequently injected with the respective nanoparticles (i.e. CR780RAD-NPs or CR780RGD-NPs) *via* the tail vein. As expected due to their ultrasmall size, these nanoparticles reached the tumor within four hours of treatment (Fig. S17). However due to their integrin $\alpha_v\beta_3$ receptor targeting ability, the CR780RGD-NPs were retained in the tumor longer than non-targeted CR780RAD-NPs. Based on these preliminary findings, we continued with the imaging of the orthotopic glioblastoma models that were injected with the respective nanoparticles (i.e. CR780RAD-NPs or CR780RGD-NPs) *via* the tail vein. Fig. 3a shows representative optoacoustic images of orthotopic brain tumors from each treatment group, acquired using the MSOT system at different time points (0 h, 4 h, 24 h) and at multiple wavelengths (680−900 nm). As observed in MSOT images from 4 h, both targeted and non-targeted nanoparticles were able to effectively reach the brain region because of the disrupted BBB (BTB), while the BBB penetration capability of CR780RGD-NPs was not evident in the normal murine brain model because of an intact BBB (Fig. S18). However, only CR780RGD-NPs were retained in the brain tumor for at least 24 h and generated a strong optoacoustic signal due to the enhanced permeability and retention effect (EPR) and active targeting. The optoacoustic signals at 4 h and 24 h were much stronger in mice treated with CR780RGD-NPs than in mice treated with CR780RAD-NPs, indicating the advantage of active targeting and long-term persistence in the bloodstream. The optoacoustic signal due to CR780 at 4 h was higher than at 24 h, indicating that some of CR780RGD-NPs undergo systemic clearance from the tumor vasculature. The optoacoustic signal was recorded in the tumor down to a depth of 5.5 mm, confirming the ability of MSOT to detect CR780RGD-NP in deep-seated brain tumors. Fig. 3b shows the optoacoustic reconstruction spectrum at different time points from the CR780RGD-NPs treated group. Spectral analysis of the brain tumor region at multiple wavelengths clearly indicates time-dependent absorption spectra changes and a strong peak at 780 nm, confirming the presence of CR780 in the region of interest. Fig. 3c shows that the signal intensity with CR780RGD-NPs is approximately 3.15- and 3.7-fold stronger than with CR780RAD-NPs at 4 h and 24 h, respectively. Fig. 3d shows optoacoustic signal intensity ratios of tumor-to-contralateral brain region, before and after treatment with CR780RAD-NPs and CR780RGD-NPs. Compared to control CR780RAD-NPs, the CR780RGD-NPs preferentially accumulated in the tumor region of the brain. These results in one mouse were confirmed in four additional mice treated with CR780RGD-NPs (Fig. S20). The tumor accumulation of CR780RGD-NPs confirms accumulation of particles due to the EPR effect and active targeting via the c(RGDyC) peptide. We compared 1 mM and 2 mM doses of CR780RGD-NPs to select the optimal concentration for brain tumor visualization. As observed in Fig. S19, tumor visualization at the 2 mM dose was poor compared to the 1 mM dose, potentially due to higher signal from the skull region (blood vessels) limiting the penetration of light. We therefore used the 1 mM dose of the NPs throughout.

To validate the results of *in vivo* MSOT based optoacoustic tomography, the brains were isolated from all animals 24 h after MSOT imaging. Optoacoustic images were acquired for isolated whole brains, and fluorescence images were acquired following brain sectioning. Fig. 4a–c

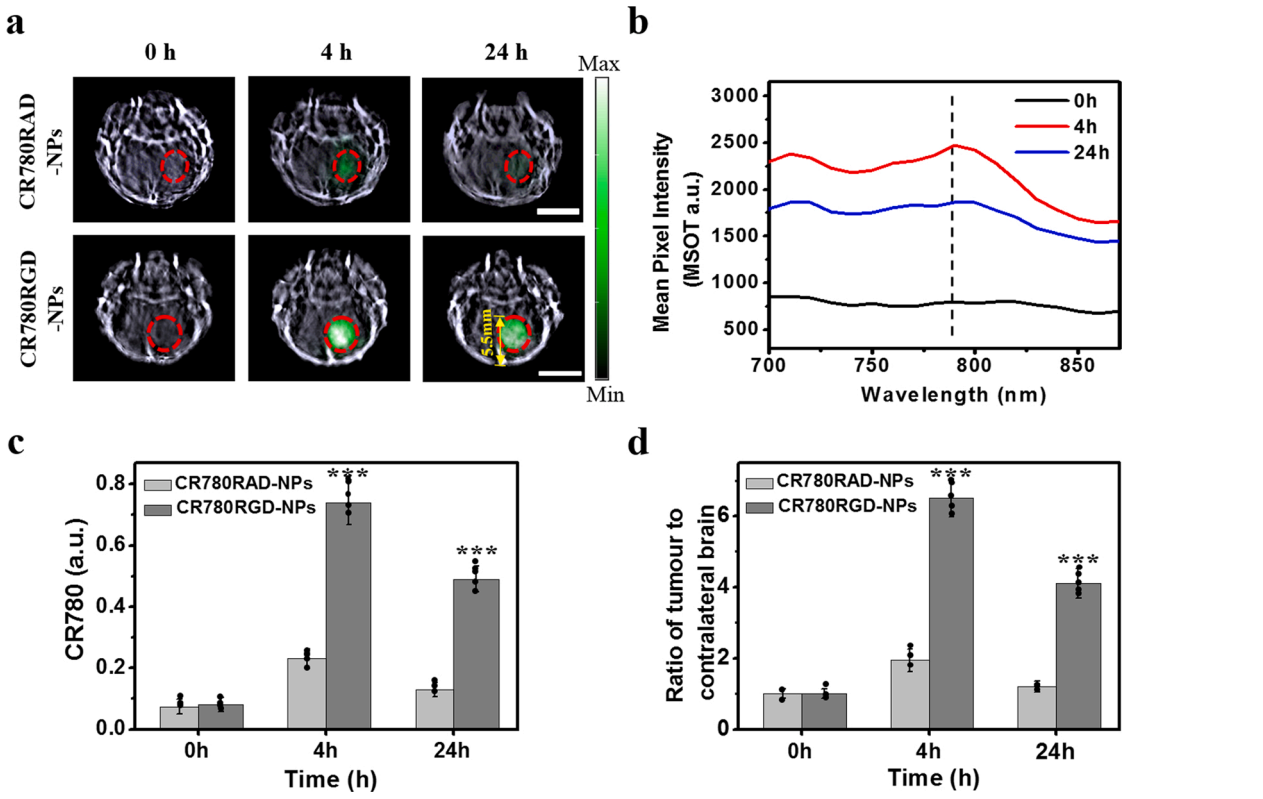

Fig. 3. *In vivo* MSOT imaging of CR780RAD-NPs and CR780RGD-NPs in a mouse brain. (a) Representative unmixed image of U87MG bearing orthotopic glioblastoma i.v. injected with 100 μL of CR780RAD-NPs or CR780RGD-NPs (1 mM). Signals are shown only for the brain tumor region (n = 5). Scale bar, 5 mm. (b) Optoacoustic spectra from the tumor region of the animal treated with CR780RGD-NPs at different time points. (c) CR780RAD-NPs and CR780RGD-NPs concentrations in the tumor region and (d) The derived optoacoustic signal intensity ratios of tumor-to-contralateral brain region, before and after treatment with CR780RAD-NPs and CR780RGD-NPs.

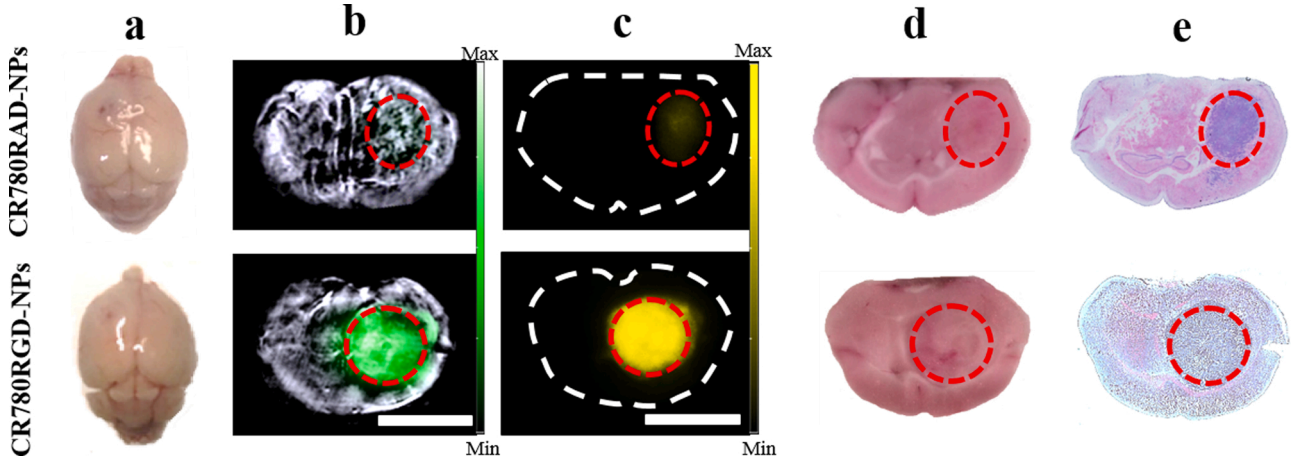

Fig. 4. (a) Photographs of representative brains isolated from tumor-bearing mice treated with CR780RAD-NPs or CR780RGD-NPs (n = 5). (b) Unmixed MSOT images of isolated brains. Scale bar, 5 mm. (c) Fluorescence images of isolated brain slices. Scale bar, 5 mm. (d, e) Bright fields and H&E staining of brain tumor slices.

and Fig. S21c show strong optoacoustic and fluorescence signals due to CR780 presence in the tumor region of mice treated with CR780RGD-NPs, while a very weak optoacoustic and fluorescence signal was observed in the isolated brains from mice treated with CR780RAD-NPs. Furthermore, the presence of the tumor in the brain was confirmed by cryo-slicing and H&E staining (Fig. 4d,e, S21).

3.6. *In vivo biodistribution and pharmacokinetics of CR780RGD-NPs*

Biodistribution of CR780RAD-NPs and CR780RGD-NPs was monitored in vital organs. After intravenous injection of the respective nanoparticles, the mice were sacrificed after 1 day and 7 days of treatment, and all vital organs were isolated and scanned using MSOT. Fig. S22 shows the optoacoustic images and signal intensities due to the presence of CR780 in different organs at day 1 and day 7. Both types of nanoparticles showed a similar level of uptake in the liver and slightly

lower uptake in the kidney, heart, and spleen at day 1. At 7 days post-injection, both nanoparticles have decreased sharply in major organs, with only little remaining in the kidney and liver. This distribution pattern is similar to that reported for organic nanoparticles, reflecting the fact that nanoparticles larger than 10 nm are cleared mainly through the hepatobiliary system [58,59]. Additionally, the pharmacokinetics of CR780RGD-NPs were evaluated from the blood clearance profile at different time points [60], which show a 11.77 h serum half-life for CR780RGD-NPs (Fig. S23).

3.7. *In vivo biosafety of CR780RGD-NPs*

To evaluate the *in vivo* safety of CR780RGD-NPs, healthy C57BL/6 mice were injected with 100 μL of CR780RGD-NPs (1 mM). The mice were sacrificed on days 1, 7, and 14 post-injection, and blood samples were collected for organ function examination (Fig. 5a, b). The blood chemistry parameters and hematology analysis results demonstrated no significant difference between mice treated with CR780RGD-NPs or PBS, and no signs of acute systemic toxicity were observed. The H&E staining and histology analysis of major organs (Fig. 5c) confirmed no noticeable nanotoxicity or damage to key organs after intravenous administration of CR780RGD-NPs. None of the treated animals died during the observation period (14 days). These results suggest that CR780RGD-NPs are well tolerated.

4. Discussion

Here we describe c(RGDyC) peptide-modified CR780 nanoparticles as highly efficient optoacoustic agents for targeted brain tumor imaging. We compared the photophysical properties of CR780RGD-NPs with those of the gold-standard FDA-approved ICG, and found that CR780RGD-NPs have an improved OGE and photostability, resulting in strong, sustained optoacoustic signals. Due to the ultrasmall size and tumor-targeting ability, CR780RGD-NPs could efficiently reach the deep-seated brain tumor to generate strong optoacoustic contrast from the targeted tumor region. Importantly, systemically injected CR780RGD-NPs show no signs of toxic side effects.

Ideal optoacoustic contrast agents should possess a low quantum

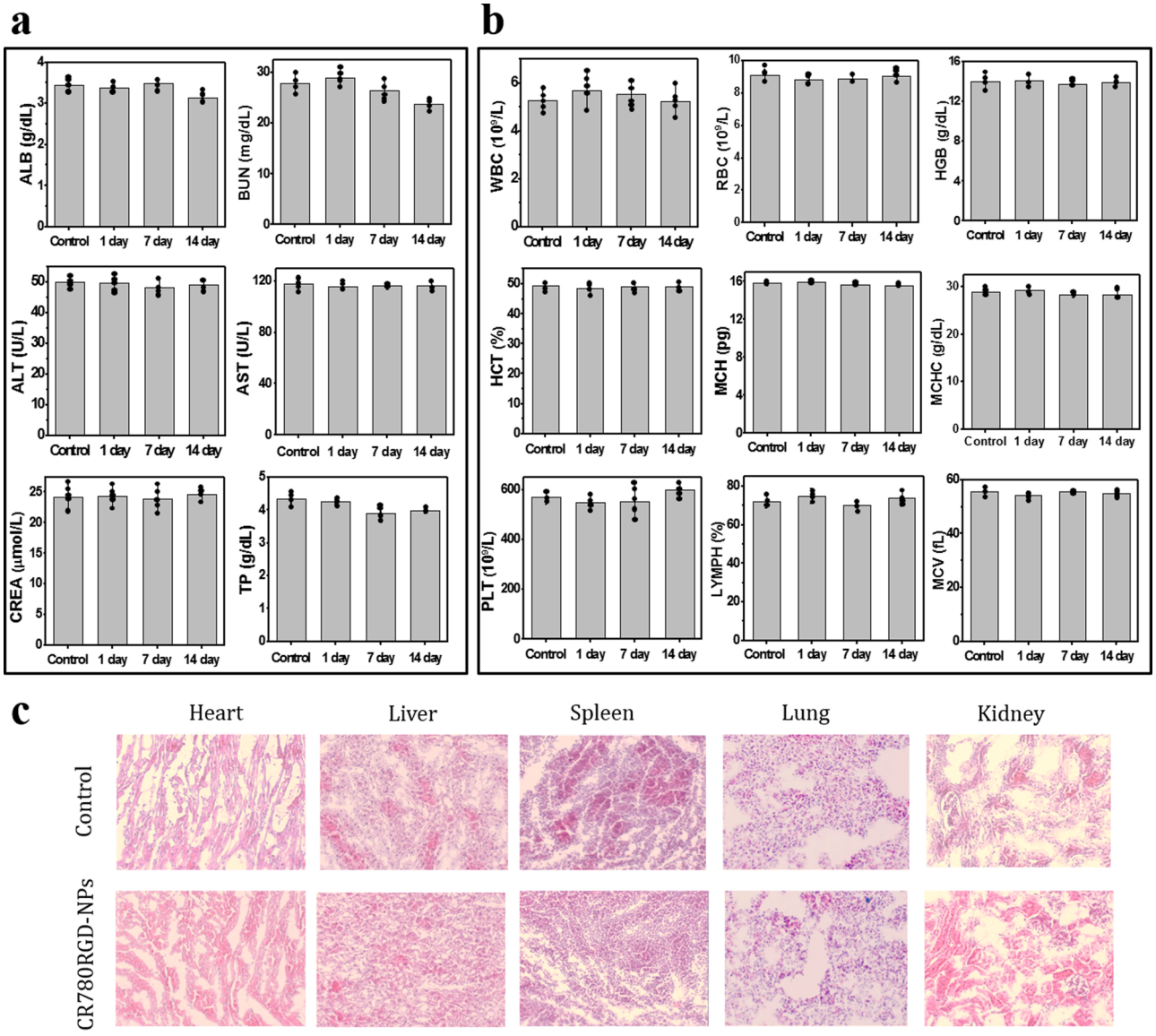

Fig. 5. Biosafety study of CR780RGD-NPs. Blood and major organs were sampled after healthy C57BL/6 mice were injected with 100 μL of CR780RGD-NPs (1 mM) or PBS (control). (a) Blood biochemistry. (b) Hematology. (c) H&E staining of vital organs (20× magnification). ALB, albumin; BUN, blood urea nitrogen; ALT, alanine transferase; AST, aspartate transferase; CREA, creatinine; TP, total protein; WBC, white blood cells; RBC, red blood cells; HGB, hemoglobin; HCT, hematocrit; MCH, mean corpuscular hemoglobin; MCHC, mean corpuscular hemoglobin concentration; PLT, platelet; LYMPH, lymphocytes; MCV, mean corpuscular volume.

yield, high molar-extinction coefficient, high OGE, narrow NIR absorption peak, and excellent photostability as well as tumor specificity and low toxicity. We found that the photostability of CR780 is very high compared to ICG under similar laser irradiation conditions, which allowed us to accurately detect the signal and quantify agents at various depths, both *in vitro* and *in vivo,* for at least 24 h. The OGE of CR780RGD-NPs is 1.8–8.5 times higher than that of the well-established NIR dyes ICG, IR780 iodide, IR820, IRDye800CW. These results clearly indicate that CR780RGD-NPs are suitable for *in vivo* optoacoustic imaging.

CR780RGD-NPs exhibit high optoacoustic signals and a high SNR, making them suitable for deep tissue imaging. Optoacoustic imaging of brain is challenging mainly due to strong optical scattering by the skull and brain tissue, which severely limits the optical fluence. Furthermore, the acoustic signals are attenuated in transit through the skull. However, CR780RGD-NPs showed a strong optoacoustic signal at a low dose and a 5 mm depth in brain tissue.

Deep-seated brain tumors are usually hard to reach because of the protection by the BBB, which normally substantially limits the brain uptake of externally administered compounds [61]. However, under disease conditions such as in cancer, the BBB is disrupted and the permeability increases, which allows nanoparticles of certain dimensions to pass through and reach different areas in the brain [33]. Nanoparticles above 100 nm in size exhibit poor brain tumor extravasation, whereas nanoparticles below 5 nm undergo rapid clearance via the kidney [62,63]. Particles in the size range of 20−70 nm are considered optimal for brain tumor targeting, with other factors such as shape, charge, and targeting activity also playing important roles [31]. We observed enhanced uptake and retention of CR780RGD-NPs (25 nm size) in the brain tumor which, when combined with active targeting via integrin $\alpha_v\beta_3$ receptors on the tumor surface, ensured a sustained optoacoustic signal from CR780 from within the tumor. The optoacoustic and fluorescence based cryo-images of isolated organs clearly indicated the accumulation of CR780RGD-NPs in the brain tumor, whereas most of the particles that did not target the tumor were safely cleared out by the liver and kidney.

The strong optoacoustic signal due to CR780RGD-NPs for at least 24 h clearly indicates the prolonged circulation time and retention of nanoparticles in the body. It was therefore important to test the biosafety and biocompatibility of the nanoparticles, and we tested the potential toxic effects due to CR780RGD-NPs treatment both *in vitro* and *in vivo*. Treatment of different concentrations of nanoparticles in U87MG cells showed no effect on cell viability. We next tested the acute toxicity of systemically injected CR780RGD-NPs in normal C57BL/6 mice for up to 14 days. The results of organ function tests and hematology clearly indicated that CR780RGD-NPs were well tolerated, and no signs of changes in blood parameters were observed throughout the observation period. Blood tests and histopathological examination suggested normal function of vital organs (heart, liver, spleen, and kidney), further confirming that the nanoparticles were well tolerated.

The multispectral optoacoustic technique MSOT allows simultaneous imaging of multiple endogenous chromophores in the brain for assessment of brain structure and function [7,51,64]. Here we extended the brain imaging abilities of MSOT by using an exogenous contrast agent that can target brain tumors and generate a strong optoacoustic signal even deep below the brain surface. The unique photophysical properties of ultrasmall CR780RGD-NPs may play a crucial role in the early diagnosis of brain tumors, identifying the margins of tumor tissue and therapy response. This is crucial for the application of MSOT and other optoacoustic techniques for diagnosis and intraoperative procedures, as well as for therapy decision-making. Our work justifies further efficacy and safety studies in large animals as a prelude to human trials.

In summary, our results show the powerful capabilities of MSOT and the developed CR780RGD-NPs for targeted optoacoustic imaging of brain tumors. The ultrasmall size of the nanoparticles ensures efficient BBB penetration, while their tumor-targeting ability, high OGE, and photostability ensure enhanced optoacoustic contrast. Biocompatible CR780RGD-NPs may be a smart diagnostic tool for integrin-expressing, deep-seated tumors and may be able to selectively deliver drugs to such tumors. This sets the foundation to explore the theranostic potential of CR780RGD-NPs as imaging agents and photothermal therapeutics against brain tumors and other cancers in the future.

Declaration of Competing Interest

V.N. is a shareholder in iThera Medical GmbH, Munich, Germany. The remaining authors declare no competing interests.

Acknowledgements

This project has received funding from the European Research Council (ERC) under the European Union's Horizon 2020 research and innovation programme under grant agreement no. 694968 (PREMSOT). The research leading to these results was supported by the Deutsche Forschungsgemeinschaft (DFG), Germany (Gottfried Wilhelm Leibniz Prize 2013, NT 3/10–1) as well as by the DFG as part of the CRC 1123 (Z1). Nian Liu acknowledges support from the China Scholarship Council. Jaya Prakash acknowledges support through the Alexander von Humboldt Postdoctoral Fellowship. We wish to thank Dr. Lin Yang, Dr. Otmar Schmid (Comprehensive Pneumology Center Munich, Institute of Lung Biology and Disease, Helmholtz Zentrum München) for helping us perform particle size measurements in their laboratory, and Dr. Doris Bengel for assisting with experimental procedures. We also wish to thank Dr. Sergey Sulima, Dr. A. Chapin Rodríguez, and Dr. Robert Wilson for helpful suggestions on the manuscript.

Appendix A. Supplementary data

Supplementary material related to this article can be found, in the online version, at doi:https://doi.org/10.1016/j.pacs.2021.100263.

References

[1] V. Ntziachristos, D. Razansky, Molecular imaging by means of multispectral optoacoustic tomography (MSOT), Chem. Rev. 110 (5) (2010) 2783–2794.
[2] V. Gujrati, A. Mishra, V. Ntziachristos, Molecular imaging probes for multi-spectral optoacoustic tomography, Chem. Commun. 53 (34) (2017) 4653–4672.
[3] S. Zackrisson, S.M.W.Y. van de Ven, S.S. Gambhir, Light in and sound out: emerging translational strategies for photoacoustic imaging, Cancer Res. 74 (4) (2014) 979–1004.
[4] A. Taruttis, V. Ntziachristos, Advances in real-time multispectral optoacoustic imaging and its applications, Nat. Photonics 9 (4) (2015) 219–227.
[5] E. Liapis, U. Klemm, A. Karlas, J. Reber, V. Ntziachristos, Resolution of spatial and temporal heterogeneity in bevacizumab-treated breast tumors by eigenspectra multispectral optoacoustic tomography, Cancer Res. 80 (23) (2020) 5291–5304.
[6] J. Li, A. Chekkoury, J. Prakash, S. Glasl, P. Vetschera, B. Koberstein-Schwarz, I. Olefir, V. Gujrati, M. Omar, V. Ntziachristos, Spatial heterogeneity of oxygenation and haemodynamics in breast cancer resolved in vivo by conical multispectral optoacoustic mesoscopy, Light Sci. Appl. 9 (1) (2020) 57.
[7] I. Olefir, A. Ghazaryan, H. Yang, J. Malekzadeh-Najafabadi, S. Glasl, P. Symvoulidis, V.B. O'Leary, G. Sergiadis, V. Ntziachristos, S.V. Ovsepian, Spatial and spectral mapping and decomposition of neural dynamics and organization of the mouse brain with multispectral optoacoustic tomography, Cell Rep. 26 (10) (2019) 2833–2846.
[8] J. Aguirre, M. Schwarz, N. Garzorz, M. Omar, A. Buehler, K. Eyerich, V. Ntziachristos, Precision assessment of label-free psoriasis biomarkers with ultra-broadband optoacoustic mesoscopy, Nat. Biomed. Eng. 1 (5) (2017) 0068.
[9] S. Tzoumas, A. Nunes, I. Olefir, S. Stangl, P. Symvoulidis, S. Glasl, C. Bayer, G. Multhoff, V. Ntziachristos, Eigenspectra optoacoustic tomography achieves quantitative blood oxygenation imaging deep in tissues, Nat. Commun. 7 (1) (2016) 12121.
[10] J. Weber, P.C. Beard, S.E. Bohndiek, Contrast agents for molecular photoacoustic imaging, Nat. Methods 13 (8) (2016) 639–650.
[11] Q. Fu, R. Zhu, J. Song, H. Yang, X. Chen, Photoacoustic imaging: contrast agents and their biomedical applications, Adv. Mater. 31 (6) (2019), 1805875.
[12] Q. Li, K. Chen, W. Huang, H. Ma, X. Zhao, J. Zhang, Y. Zhang, C. Fang, L. Nie, Minimally invasive photothermal ablation assisted by laparoscopy as an effective preoperative neoadjuvant treatment for orthotopic hepatocellular carcinoma, Cancer Lett. 496 (2021) 169–178.
[13] X. Huang, M.A. El-Sayed, Gold nanoparticles: optical properties and implementations in cancer diagnosis and photothermal therapy, J. Adv. Res. 1 (1) (2010) 13–28.

[14] Y.F. Li, C. Chen, Fate and toxicity of metallic and metal-containing nanoparticles for biomedical applications, Small 7 (21) (2011) 2965–2980.
[15] Y. Cai, W. Si, W. Huang, P. Chen, J. Shao, X. Dong, Organic dye based nanoparticles for Cancer phototheranostics, Small 14 (25) (2018), 1704247.
[16] A. Nunes, V.J. Pansare, N. Beziere, A.K. Ntoukas, J. Reber, M. Bruzek, J. Anthony, R.K. Prud'homme, V. Ntziachristos, Quenched hexacene optoacoustic nanoparticles, J. Mater. Chem. B 6 (1) (2018) 44–55.
[17] N. Beziere, N. Lozano, A. Nunes, J. Salichs, D. Queiros, K. Kostarelos, V. Ntziachristos, Dynamic imaging of PEGylated indocyanine green (ICG) liposomes within the tumor microenvironment using multi-spectral optoacoustic tomography (MSOT), Biomaterials 37 (2015) 415–424.
[18] S. Sreejith, J. Joseph, M. Lin, N.V. Menon, P. Borah, H.J. Ng, Y.X. Loong, Y. Kang, S.W.-K. Yu, Y. Zhao, Near-infrared squaraine dye encapsulated micelles for in vivo fluorescence and photoacoustic bimodal imaging, ACS Nano 9 (6) (2015) 5695–5704.
[19] F.P. Gao, Y.X. Lin, L.L. Li, Y. Liu, U. Mayerhoffer, P. Spenst, J.G. Su, J.Y. Li, F. Wurthner, H. Wang, Supramolecular adducts of squaraine and protein for noninvasive tumor imaging and photothermal therapy in vivo, Biomaterials 35 (3) (2014) 1004–1014.
[20] T. Kowada, H. Maeda, K. Kikuchi, BODIPY-based probes for the fluorescence imaging of biomolecules in living cells, Chem. Soc. Rev. 44 (14) (2015) 4953–4972.
[21] E.S. Nyman, P.H. Hynninen, Research advances in the use of tetrapyrrolic photosensitizers for photodynamic therapy, J. Photochem. Photobiol. B Biol. 73 (1) (2004) 1–28.
[22] D.E. Lynch, D.G. Hamilton, Croconaine dyes - the lesser known siblings of Squaraines, Eur. J. Org. Chem. 2017 (27) (2017) 3897–3911.
[23] S. Ye, C. Zhang, J. Mei, Z. Li, S. Xu, X. Li, C. Yao, A highly selective optical probe for sensing of Fe^{3+} based on a water-soluble croconaine, J. Photochem. Photobiol. A 347 (2017) 130–137.
[24] L. Liu, M.H. Liu, L.L. Deng, B.P. Lin, H. Yang, Near-infrared chromophore functionalized Soft actuator with ultrafast photoresponsive speed and superior mechanical property, J. Am. Chem. Soc. 139 (33) (2017) 11333–11336.
[25] Y. Liu, Y. Yang, M. Sun, M. Cui, Y. Fu, Y. Lin, Z. Li, L. Nie, Highly specific noninvasive photoacoustic and positron emission tomography of brain plaque with functionalized croconium dye labeled by a radiotracer, Chem. Sci. 8 (4) (2017) 2710–2716.
[26] S. Lei, Y. Zhang, N.T. Blum, P. Huang, J. Lin, Recent advances in Croconaine Dyes for bioimaging and theranostics, Bioconjug. Chem. 31 (9) (2020) 2072–2084.
[27] S. Guha, G.K. Shaw, T.M. Mitcham, R.R. Bouchard, B.D. Smith, Croconaine rotaxane for acid activated photothermal heating and ratiometric photoacoustic imaging of acidic pH, Chem. Commun. 52 (1) (2016) 120–123.
[28] Q. Chen, X. Liu, J. Zeng, Z. Cheng, Z. Liu, Albumin-NIR dye self-assembled nanoparticles for photoacoustic pH imaging and pH-responsive photothermal therapy effective for large tumors, Biomaterials 98 (2016) 23–30.
[29] L. Tang, F. Zhang, F. Yu, W. Sun, M. Song, X. Chen, X. Zhang, X. Sun, Croconaine nanoparticles with enhanced tumor accumulation for multimodality cancer theranostics, Biomaterials 129 (2017) 28–36.
[30] Y. Liu, H. Liu, H. Yan, Y. Liu, J. Zhang, W. Shan, P. Lai, H. Li, L. Ren, Z. Li, L. Nie, Aggregation-induced absorption enhancement for deep near-infrared II photoacoustic imaging of brain gliomas in vivo, Adv. Sci. 6 (8) (2019), 1801615.
[31] W. Tang, W. Fan, J. Lau, L. Deng, Z. Shen, X. Chen, Emerging blood-brain-barrier-crossing nanotechnology for brain cancer theranostics, Chem. Soc. Rev. 48 (11) (2019) 2967–3014.
[32] L. Chen, D. Zeng, N. Xu, C. Li, W. Zhang, X. Zhu, Y. Gao, P.R. Chen, J. Lin, Blood-brain barrier- and blood-brain tumor barrier-penetrating peptide-derived targeted therapeutics for glioma and malignant tumor brain metastases, ACS Appl. Mater. Interfaces 11 (45) (2019) 41889–41897.
[33] C.D. Arvanitis, G.B. Ferraro, R.K. Jain, The blood–brain barrier and blood–tumour barrier in brain tumours and metastases, Nat. Rev. Cancer 20 (1) (2020) 26–41.
[34] V. Ceña, P. Játiva, Nanoparticle crossing of blood–brain barrier: a road to new therapeutic approaches to central nervous system diseases, Nanomedicine 13 (13) (2018) 1513–1516.
[35] J.W. Seo, J. Ang, L.M. Mahakian, S. Tam, B. Fite, E.S. Ingham, J. Beyer, J. Forsayeth, K.S. Bankiewicz, T. Xu, K.W. Ferrara, Self-assembled 20-nm ^{64}Cu-micelles enhance accumulation in rat glioblastoma, J. Control. Release 220 (Pt A) (2015) 51–60.
[36] M.F. Kircher, A. de la Zerda, J.V. Jokerst, C.L. Zavaleta, P.J. Kempen, E. Mittra, K. Pitter, R. Huang, C. Campos, F. Habte, R. Sinclair, C.W. Brennan, I. K. Mellinghoff, E.C. Holland, S.S. Gambhir, A brain tumor molecular imaging strategy using a new triple-modality MRI-photoacoustic-Raman nanoparticle, Nat. Med. 18 (5) (2012) 829–834.
[37] C. Liu, S. Li, Y. Gu, H. Xiong, W.T. Wong, L. Sun, Multispectral photoacoustic imaging of tumor protease activity with a gold nanocage-based activatable probe, Mol. Imaging Biol. 20 (6) (2018) 919–929.
[38] C. Liu, J. Chen, Y. Zhu, X. Gong, R. Zheng, N. Chen, D. Chen, H. Yan, P. Zhang, H. Zheng, Z. Sheng, L. Song, Highly sensitive MoS_2-Indocyanine green hybrid for photoacoustic imaging of orthotopic brain glioma at deep site, Nano-micro lett. 10 (3) (2018) 48.
[39] J. Chen, C. Liu, D. Hu, F. Wang, H. Wu, X. Gong, X. Liu, L. Song, Z. Sheng, H. Zheng, Single-layer MoS2Nanosheets with amplified photoacoustic effect for highly sensitive photoacoustic imaging of orthotopic brain tumors, Adv. Funct. Mater. 26 (47) (2016) 8715–8725.
[40] K. Pu, A.J. Shuhendler, J.V. Jokerst, J. Mei, S.S. Gambhir, Z. Bao, J. Rao, Semiconducting polymer nanoparticles as photoacoustic molecular imaging probes in living mice, Nat. Nanotechnol. 9 (3) (2014) 233–239.
[41] K. Rurack, M. Spieles, Fluorescence quantum yields of a series of red and near-infrared dyes emitting at 600-1000 nm, Anal. Chem. 83 (4) (2011) 1232–1242.
[42] C. Würth, M. Grabolle, J. Pauli, M. Spieles, U. Resch-Genger, Comparison of methods and achievable uncertainties for the relative and absolute measurement of photoluminescence quantum yields, Anal. Chem. 83 (9) (2011) 3431–3439.
[43] J.P. Fuenzalida Werner, Y. Huang, K. Mishra, R. Janowski, P. Vetschera, C. Heichler, A. Chmyrov, C. Neufert, D. Niessing, V. Ntziachristos, A.C. Stiel, Anal. Chem. 92 (15) (2020) 10717–10724.
[44] N. Liu, P. O'Connor, V. Gujrati, D. Gorpas, S. Glasl, A. Blutke, A. Walch, K. Kleigrewe, M. Sattler, O. Plettenburg, V. Ntziachristos, Facile synthesis of a croconaine-based nanoformulation for optoacoustic imaging and photothermal therapy, Adv. Healthc. Mater. (2021) 2002115.
[45] X. Song, J.W. Foley, A new water-soluble near-infrared croconium dye, Dyes Pigm. 78 (1) (2008) 60–64.
[46] M. Lepore, I. Delfino, Intralipid-based phantoms for the development of new optical diagnostic techniques, Open Biotechnol. J. 13 (1) (2019) 163–172.
[47] A. Rehman, I. Ahmad, K. Rehman, S. Anwar, S. Firdous, M. Nawaz, Optical properties measurement of highly diffusive tissue phantoms for biomedical applications, Laser Phys. 25 (2) (2015), 025605.
[48] D. Ni, J. Zhang, W. Bu, H. Xing, F. Han, Q. Xiao, Z. Yao, F. Chen, Q. He, J. Liu, S. Zhang, W. Fan, L. Zhou, W. Peng, J. Shi, Dual-targeting upconversion nanoprobes across the blood–Brain barrier for magnetic Resonance/Fluorescence imaging of intracranial glioblastoma, ACS Nano 8 (2) (2014) 1231–1242.
[49] V. Gujrati, M. Lee, Y.-J. Ko, S. Lee, D. Kim, H. Kim, S. Kang, S. Lee, J. Kim, H. Jeon, Bioengineered yeast-derived vacuoles with enhanced tissue-penetrating ability for targeted cancer therapy, Proc. Natl. Acad. Sci. 113 (3) (2016) 710–715.
[50] Y. Song, D. Du, L. Li, J. Xu, P. Dutta, Y.H. Lin, In vitro study of receptor-mediated silica nanoparticles delivery across blood-brain barrier, ACS Appl. Mater. Interfaces 9 (24) (2017) 20410–20416.
[51] N.C. Burton, M. Patel, S. Morscher, W.H. Driessen, J. Claussen, N. Beziere, T. Jetzfellner, A. Taruttis, D. Razansky, B. Bednar, V. Ntziachristos, Multispectral opto-acoustic tomography (MSOT) of the brain and glioblastoma characterization, NeuroImage 65 (2013) 522–528.
[52] M.D. Laramie, M.K. Smith, F. Marmarchi, L.R. McNally, M. Henary, Small molecule optoacoustic contrast agents: an unexplored avenue for enhancing in vivo imaging, Molecules 23 (11) (2018) 2766.
[53] Z. Chen, X.L. Dean-Ben, S. Gottschalk, D. Razansky, Performance of optoacoustic and fluorescence imaging in detecting deep-seated fluorescent agents, Biomed. Opt. Express 9 (5) (2018) 2229–2239.
[54] P. Huang, P. Rong, A. Jin, X. Yan, M.G. Zhang, J. Lin, H. Hu, Z. Wang, X. Yue, W. Li, G. Niu, W. Zeng, W. Wang, K. Zhou, X. Chen, Dye-loaded ferritin nanocages for multimodal imaging and photothermal therapy, Adv. Mater. 26 (37) (2014) 6401–6408.
[55] L. Wang, P.P. Yang, X.X. Zhao, H. Wang, Self-assembled nanomaterials for photoacoustic imaging, Nanoscale 8 (5) (2016) 2488–2509.
[56] S. Liu, Radiolabeled cyclic RGD peptides as integrin alpha(v)beta(3)-targeted radiotracers: maximizing binding affinity via bivalency, Bioconjug. Chem. 20 (12) (2009) 2199–2213.
[57] D. Razansky, J. Baeten, V. Ntziachristos, Sensitivity of molecular target detection by multispectral optoacoustic tomography (MSOT), Med. Phys. 36 (3) (2009) 939–945.
[58] Y.-N. Zhang, W. Poon, A.J. Tavares, I.D. McGilvray, W.C.W. Chan, Nanoparticle–liver interactions: cellular uptake and hepatobiliary elimination, J. Control. Release 240 (2016) 332–348.
[59] M. Longmire, P.L. Choyke, H. Kobayashi, Clearance properties of nano-sized particles and molecules as imaging agents: considerations and caveats, Nanomedicine 3 (5) (2008) 703–717.
[60] P. Chen, Y. Ma, Z. Zheng, C. Wu, Y. Wang, G. Liang, Facile syntheses of conjugated polymers for photothermal tumour therapy, Nat. Commun. 10 (1) (2019) 1192.
[61] P.K. Pandey, A.K. Sharma, U. Gupta, Blood brain barrier: an overview on strategies in drug delivery, realistic in vitro modeling and in vivo live tracking, Tissue Barriers 4 (1) (2016), e1129476.
[62] N. Hoshyar, S. Gray, H. Han, G. Bao, The effect of nanoparticle size on in vivo pharmacokinetics and cellular interaction, Nanomedicine 11 (6) (2016) 673–692.
[63] D. Furtado, M. Bjornmalm, S. Ayton, A.I. Bush, K. Kempe, F. Caruso, Overcoming the blood-brain barrier: the role of nanomaterials in treating neurological diseases, Adv. Mater. (2018), 1801362.
[64] S.J. Park, C.J.H. Ho, S. Arai, A. Samanta, M. Olivo, Y.T. Chang, Visualizing alzheimer's disease mouse brain with multispectral optoacoustic tomography using a fluorescent probe, CDnir7, Sci. Rep. 9 (1) (2019) 12052.

Nian Liu is currently a Ph.D. student in the Institute for Biological and Medical Imaging (IBMI) at Technical University of Munich and Helmholtz Zentrum München, Germany. He received his M.Sc from Wuhan University of Technology, China. His research interests are optical contrast agents for cancer theranostics.

Dr. Vipul Gujrati received his Master's in Pharmacy in 2006 from the Rajiv Gandhi University of Health Sciences in India, after which he worked as a research scientist at Torrent Pharmaceuticals LTD in India. From 2010–2014, he completed a PhD on the development of bioengineered drug delivery nanocarriers under the guidance of Prof. Dr Sangyong Jon at the Gwangju Institute of Science and Technology (GIST) and Korea Advanced Institute of Science and Technology (KAIST) in South Korea, where he stayed on as a postdoctoral researcher. In May 2016 he joined the group of Prof. Dr Vasilis Ntziachristos at the Institute for Biological and Medical Imaging (IBMI) at the Technical University of Munich (TUM), Germany, as a postdoctoral fellow. At IBMI he is developing and studying biological and synthetic nano-carrier-probes for optoacoustic imaging and drug delivery. His research interests relate to the development of multifunctional nano-carriers for sensing, imaging and drug delivery. One of his aims is to develop novel nano-based tools to understand the pathobiology of disease as well as to improve disease diagnosis, drug delivery, and therapy monitoring.

Professor Vasilis Ntziachristos studied Electrical Engineering at Aristotle University in Thessaloniki, Greece and received his M.Sc. and Ph.D. from the Bioengineering Department of the University of Pennsylvania. He served as assistant professor and director of the Laboratory for Bio-Optics and Molecular Imaging at Harvard University and Massachusetts General Hospital. Currently, he is the Director of the Institute for Biological and Medical Imaging at the Helmholtz Zentrum in Munich, Germany, as well as a Professor of Electrical Engineering, Professor of Medicine and Chair for Biological Imaging at the Technical University Munich, Germany. His work focuses on novel innovative optical and optoacoustic imaging modalities for studying biological processes and diseases as well as the translation of these findings into the clinic.